PHYSICAL REVIEW B **84**, 140103(R) (2011)

Coherent solid/liquid interface with stress relaxation in a phase-field approach to the melting/solidification transition

Valery I. Levitas[1] and Kamran Samani[2]

[1]*Iowa State University, Departments of Aerospace Engineering, Mechanical Engineering, and Material Science and Engineering, Ames, Iowa 50011, USA*

[2]*Iowa State University, Department of Mechanical Engineering, Ames, Iowa 50011, USA*

(Received 13 June 2011; revised manuscript received 21 August 2011; published 21 October 2011)

An advanced Ginzburg-Landau (GL) approach to melting and solidification coupled with mechanics is developed. It is based on the concept of a coherent solid-liquid interface with a transformation strain tensor, the deviatoric part of which is described by a thermodynamically consistent kinetic equation. Due to the relaxation of the elastic energy, a promoting contribution to the driving force for phase transformation in the GL equation appears, both for melting and solidification. Good agreement with known experiments is obtained for Al nanoparticles for the size-dependent melting temperature and temperature-dependent thickness of the surface molten layer. All types of interface stress distributions from known molecular dynamics simulations are obtained and interpreted. A similar approach can be applied for sublimation and condensation, amorphization and vitrification, diffusive transformations, and chemical reactions.

DOI: 10.1103/PhysRevB.84.140103 PACS number(s): 64.70.Nd, 64.70.dj

Stresses within a few-nanometer-thick interface currently have become a separate topic of interest in the thermodynamic and molecular dynamics (MD) approaches[1] to melting because they affect significantly the thermodynamics and kinetics of melting. However, they were not studied in the phase-field or Ginzburg-Landau (GL) approaches. While the GL approach is widely used to model premelting[2] and melting,[3] mechanical issues have been addressed only recently for premelting[4] and melting.[4,5] Thus, models for a coherent solid-melt interface without[5] and with[4] surface tension were developed. However, the outstanding problem is related to the transformation strain tensor $\boldsymbol{\varepsilon}_t$ that transforms the elemental volume of one phase into another in an unloaded state. For martensitic phase transformations, $\boldsymbol{\varepsilon}_t = 1/3\varepsilon_{0t}\boldsymbol{I} + \boldsymbol{e}_t$ transforms the crystal lattice of austenite into a lattice of martensite—i.e., the entire tensor is completely determined when lattices are known. Here, ε_{0t} is the volumetric transformation strain, $\boldsymbol{I}$ is the unit tensor, and $\boldsymbol{e}_t$ is the deviatoric transformation strain that characterizes the change in shape. For melting and solidification, only the change in specific volume (or density) is known, and it was always assumed that the pure volumetric transformation strain $\boldsymbol{\varepsilon}_t = 1/3\varepsilon_{0t}\boldsymbol{I}$ and $\boldsymbol{e}_t = 0$. Such an assumption works well for sharp interface approaches.[6] However, for a coherent, finite-width interface in the GL approach, pure volumetric transformation strain generates huge internal elastic stresses, which yield multiple contradictions with available experimental and MD results (see Figs. 1–4 below and Ref. 4). Thus, the melting temperature for an Al nanoparticle with a radius $R > 20$ nm is becoming larger than the bulk equilibrium melting temperature θ_e (Fig. 1). The relationship between the thickness of the surface molten layer h versus temperature θ for $R > 40$ nm is qualitatively different from experiments (Fig. 2). The interface stresses are an order of magnitude larger than in MD simulations[1] and may have an opposite sign [Fig. 3(b)]. And finally, internal stresses lead to an overestimation of the interface velocity (Fig. 4). These contradictions show the necessity of introducing and defining the deviatoric transformation strain $\boldsymbol{e}_t$, which will lead to stress relaxation. The fact that it is unknown from a geometric consideration does not mean it should be zero. Atoms during transformations can move in a way that reduces elastic energy and increases the driving force for transformation; this results in some deviatoric transformation strain in a continuum description. In this Rapid Communication, we expanded the phase-field theory for melting by developing thermodynamically consistent kinetic equations for $\boldsymbol{e}_t$. This also results in an additional contribution to the driving force for melting in the GL equation. The theory is applied for resolving all of the above contradictions in melting and premelting of Al nanosize and large-size particles. Results are in good agreement with experiments for the melting temperature versus R and the thickness of the molten layer versus θ, as well reproducing all types of distributions of interface stresses obtained with MD.

We designate the contractions of tensors $\boldsymbol{A}$ and $\boldsymbol{B}$ over one and two indices as $\boldsymbol{A}\cdot\boldsymbol{B}$ and $\boldsymbol{A}:\boldsymbol{B}$, respectively; $\otimes$ designates a dyadic product, and $\overset{\circ}{\nabla}$ and ∇ are the gradients in the undeformed and deformed states. The subscripts or superscripts e, t, and θ are for elastic, transformational, and thermal contributions to energy, strain, and stress; subscripts st and $*$ are for the surface tension and symmetrization, and $\Delta A = A_s - A_m$ is for any property A, with subscripts s and m for solid and melt.

Model. We will further develop our model with a coherent solid-melt interface from Ref. 4. For simplicity, viscosity is neglected and shear strain is small. Melting is described with the help of the order parameter η that varies from 1 in solid to 0 in melt. We will use the decomposition of strain $\boldsymbol{\varepsilon} = 1/3\varepsilon_0\boldsymbol{I} + \boldsymbol{e}$ and stress $\boldsymbol{\sigma} = p\boldsymbol{I} + \boldsymbol{S}$ tensors into spherical and deviatoric parts with $p = \boldsymbol{\sigma}:\boldsymbol{I}/3$ for mean stress and ε_0 for volumetric strain. The standard relationship for strain $\boldsymbol{\varepsilon} = (\overset{\circ}{\nabla}\boldsymbol{u})_*$ in terms of displacements $\boldsymbol{u}$ and equilibrium equations $\nabla\cdot\boldsymbol{\sigma} = \boldsymbol{0}$ is used. The distinguished point in kinematic decomposition

$$\boldsymbol{\varepsilon} = \boldsymbol{\varepsilon}_e + \boldsymbol{\varepsilon}_t + \boldsymbol{\varepsilon}_\theta, \quad \boldsymbol{\varepsilon}_t = 1/3\varepsilon_{0t}(1-\phi(\eta))\boldsymbol{I} + \boldsymbol{e}_t, \qquad (1)$$

with $\boldsymbol{\varepsilon}_\theta = [\alpha_m + \Delta\alpha\phi(\eta)](\theta - \theta_e)\boldsymbol{I}$ and $\phi(\eta) = \eta^2(3 - 2\eta)$ is the introduction of the deviatoric transformation strain $\boldsymbol{e}_t$ for melting, which is defined by a thermodynamically consistent kinetic equation (derived below)

$$\dot{\boldsymbol{e}}_t = 6\Lambda\eta(1 - \eta)\boldsymbol{S}_e|\varepsilon_{0t}||\dot{\eta}|, \tag{2}$$

where α is the linear thermal expansion coefficient and $\Lambda \geqslant 0$ is the kinetic coefficient. The Helmholtz free energy per unit undeformed volume of solid ψ and its contributions are

$$\begin{aligned}
\psi &= \psi^e(\varepsilon_0, \boldsymbol{e}, \eta, \theta) + J\check{\psi}^\theta + \psi^\theta + J\psi^\nabla, \\
J &= \rho_0/\rho = 1 + \varepsilon_0, \\
\psi^e &= 0.5[K_m + \Delta K\phi(\eta)]\varepsilon_{0e}^2 + \mu\phi(\eta)\boldsymbol{e}_e : \boldsymbol{e}_e, \\
\psi^\theta &= H(\theta/\theta_e - 1)\phi(\eta), \quad \check{\psi}^\theta = A\eta^2(1 - \eta)^2, \\
\psi^\nabla &= 0.5\beta|\nabla\eta|^2, \quad A := 3H(1 - \theta_c/\theta_e).
\end{aligned} \tag{3}$$

Here, ρ_0 and ρ are the mass densities in the nondeformed and deformed states, K and μ are the bulk and shear modulus, β is the gradient energy coefficient, H is the heat of fusion, $\check{\psi}^\theta$ is the double-well energy, and θ_c is the melt instability temperature. Despite the small strain approximation, one cannot simplify $J \simeq 1$ and $\nabla \simeq \overset{\circ}{\nabla}$, because in this case surface tension disappears. For such an energy, expressions for stress and the GL equation are

$$\boldsymbol{\sigma} = \frac{\partial\psi}{\partial\boldsymbol{\varepsilon}} - J^{-1}\nabla\eta \otimes \frac{\partial\psi}{\partial\nabla\eta} = \boldsymbol{\sigma}_e + \boldsymbol{\sigma}_{\mathrm{st}}, \tag{4}$$

$$\begin{aligned}
\boldsymbol{\sigma}_e &= [K_m + \Delta K\phi(\eta)]\varepsilon_{0e}\boldsymbol{I} + 2\mu\phi(\eta)\boldsymbol{e}_e, \\
\sigma_{\mathrm{st}} &= (\psi^\nabla + \check{\psi}_\theta)\boldsymbol{I} - \beta\nabla\eta \otimes \nabla\eta,
\end{aligned} \tag{5}$$

$$\begin{aligned}
\frac{1}{\chi}\dot{\eta} = X_\eta &= -J^{-1}\left.\frac{\partial\psi}{\partial\eta}\right|_{\boldsymbol{\varepsilon}} + \nabla \cdot \left(J^{-1}\frac{\partial\psi}{\partial\nabla\eta}\right) \\
&= \beta\nabla^2\eta - 6J^{-1}[H(\theta/\theta_e - 1) + p_e\varepsilon_{0t} - \Lambda|\varepsilon_{0t}| \\
&\quad \times \boldsymbol{S}_e : \boldsymbol{S}_e \operatorname{sign}(\dot{\eta}) - 3p_e\Delta\alpha(\theta - \theta_e) + 0.5\Delta K\varepsilon_{0e}^2 \\
&\quad + \mu\boldsymbol{e}_e : \boldsymbol{e}_e]\eta(1 - \eta) - 4A\eta(1 - \eta)(0.5 - \eta),
\end{aligned} \tag{6}$$

where χ is the coefficient and X_η is the driving force for changing in η, determined from the expression for the dissipation rate $D = X_\eta\dot{\eta} \geqslant 0$. Because of the introduction of a deviatoric transformation strain in Eq. (2), an additional promoting (for both melting and solidification) contribution to X_η, $6J^{-1}\Lambda|\varepsilon_{0t}|\boldsymbol{S}_e{:}\boldsymbol{S}_e \operatorname{sign}(\dot{\eta})$, appears. Because of this term, even a stationary solution of Eq. (6) for η depends on Λ; due to Eq. (2), it depends on the entire evolution of $\boldsymbol{S}_e$ and $\boldsymbol{e}_t$ toward their stationary solutions. The coupled Eqs. (1)–(6) are solved for all problems below using the finite element method (FEM) code COMSOL.

To outline the derivation of Eq. (2) and its contribution to the GL Eq. (6), we can neglect surface stresses and the dependence of ψ on $\nabla\eta$, and put $J \simeq 1$ for brevity; the final results are the same. Substituting ψ and Eq. (1) in the expression for the dissipation rate $D = \boldsymbol{\sigma}_e : \dot{\boldsymbol{\varepsilon}} - \dot{\psi} \geqslant 0$, and using the independence of D of $\dot{\boldsymbol{\varepsilon}}_e$ and $\dot{\theta}$, one obtains Eq. (4) and $D = [p_e\varepsilon_{0t}\phi'(\eta) - \frac{\partial\psi}{\partial\eta}]\dot{\eta} + \boldsymbol{S}_e : \dot{\boldsymbol{e}}_t \geqslant 0$. To allow change in $\boldsymbol{e}_t$ during transformation only, we put $\dot{\boldsymbol{e}}_t = 0$ for $\dot{\eta} = 0$. We also would like to impose that the equation for $\dot{\boldsymbol{e}}_t$ is the same for both direct and reverse transformations. Then, in general, $\dot{\boldsymbol{e}}_t = f(\boldsymbol{S}_e, \eta, |\dot{\eta}|)$. Inequality $D \geqslant 0$ should be satisfied for all possible processes. Choosing p_e that satisfies $p_e\varepsilon_{0t}\phi'(\eta) = \frac{\partial\psi}{\partial\eta}$ at least for one time instant, one obtains $\boldsymbol{S}_e : \dot{\boldsymbol{e}}_t \geqslant 0$. The equation $\dot{\boldsymbol{e}}_t = \Lambda|\varepsilon_{0t}\dot{\phi}(\eta)|\boldsymbol{S}_e$ with $\Lambda \geqslant 0$ is the simplest one that satisfies all of the above conditions and also scales $\dot{\boldsymbol{e}}_t$ with the rate of volumetric transformation strain. It coincides with Eq. (2). Since $|\dot{\eta}| = \dot{\eta}\operatorname{sign}(\dot{\eta})$, the substitution of Eq. (2) in D results in an $\boldsymbol{S}_e$ related term $6\Lambda|\varepsilon_{0t}|\boldsymbol{S}_e : \boldsymbol{S}_e\eta(1 - \eta)\operatorname{sign}(\dot{\eta})\dot{\eta}$, which justifies that X_η should have the contribution shown in Eq. (6). During transformation, the evolution of $\boldsymbol{e}_t$ relaxes elastic deviatoric stress $\boldsymbol{S}_e$ and elastic energy, and this relaxation produces a promoting contribution to X_η for both melting and solidification. Note that Eq. (2) leads to the maximization of the magnitude of the driving force X_η, which is in line with the postulate of realizability.[7]

The thermodynamic procedure[11] that led to GL equation, also results in the boundary conditions:[4]

$$\begin{aligned}
J\frac{\partial\psi}{\partial\nabla\eta} \cdot \boldsymbol{n} = \beta\nabla\eta \cdot \boldsymbol{n} &= -\frac{d\gamma}{d\eta}, \quad \gamma(\eta) = \gamma_l + (\gamma_s - \gamma_l)\phi(\eta), \\
\sigma_n &= -\frac{2\gamma(\eta)}{R} - \bar{p},
\end{aligned} \tag{7}$$

where $\boldsymbol{n}$ is the unit normal to the boundary; $\gamma(\eta)$ is the specific surface energy with γ_l and γ_s for the surface energy of liquid and solid, respectively; σ_n is the normal to interface stress; $1/R$ is the mean curvature, and $\bar{p}$ is the external pressure ($\bar{p} = 0$ in simulations). If surface energy does not change during melting, then $\gamma = \text{const}$ and Eq. (7) reduces to traditional boundary condition $\nabla\eta \cdot \boldsymbol{n} = 0$. As initial conditions, values of η and $\boldsymbol{e}_t$ in the entire volume are 0.99 and 0, respectively. For the interface velocity and its dependence on heating rate in Fig. 3, homogeneous temperature is prescribed by equation $\theta = 890K + (\text{heating rate})\,t$, where t is time in seconds.

We use the following material parameters for Al obtained for macroscopic sample:[4,8–10] $\theta_e = 933.67K$, $H = 933.57 \times 10^6$ J/m^3, $K_m = 41.3$ GPa, $K_s = 71.1$ GPa, $\mu = 27.3$ GPa, $\varepsilon_{0t} = 0.06, \alpha_m = 4.268 \times 10^{-5}$ K^{-1}, $\alpha_s = 3.032 \times 10^{-5}$ K^{-1}, $\gamma_s = 1.050$ J/m^2, $\gamma_l = 0.931$ J/m^2, $\beta = 3.21 \times 10^{-10}$ N (which results in solid-liquid interface energy $\gamma_{sl} = 0.1$ J/m^2), $\chi = 400$ m^2/Ns, $\theta_c/\theta_e = 0.8$ (which leads to $\theta_i/\theta_e = 1.2$, $\theta_c = 746.9$ K, and the solid instability temperature $\theta_i = 1120.4$ K). For particles of radius R, homogeneously increasing temperature is prescribed, and stationary solutions have been determined for each temperature. The interface position corresponds to the point with $\eta = 0.5$. The thickness h of a premolten and completely liquid surface layer was determined and plotted as a function of $\theta_e - \theta$ (Fig. 2). The melting temperature θ_m is defined as the temperature at which the stationary, two-phase solution loses its stability and the interface propagates to the center.

Results. In Fig. 1(a), the melting temperatures for models without ($\Lambda = 0$) and with ($\Lambda = 4 \times 10^{-2}$) deviatoric transformation strain are compared with experimental results; here and below Λ is in MPa^{-1}. This value of Λ represents the smallest one, above which θ_m does not practically reduce and $\theta_m = \theta_e$ for $R \to \infty$. For particles with $R < 10$ nm, surprisingly, both models yield an equal melting temperature. For larger particles, neglecting deviatoric transformation strain introduces large internal elastic stresses that suppress melting, and consequently, melting temperatures are larger. For $R > 20$ nm and $\Lambda = 0$, the melting temperature becomes

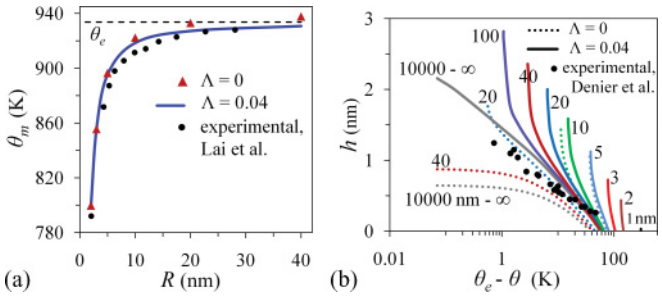

FIG. 1. (Color online) (a) Size dependence of melting temperature for Al nanoparticles for two different values of Λ (in MPa^{-1}) vs experimental data (Ref. 8) (dots). (b) Temperature dependence of the thickness of the molten surface for Al for different particle radii (shown in nm near curves) and values of Λ vs experimental data (Ref. 9) (dots).

larger than θ_e, which is contradictory and shows that such a model cannot be used. The model with deviatoric strain corresponds well to experiments. Note that internal stresses for $\Lambda = 0$ are mostly due to the tangential component $\varepsilon_{t\phi} = \varepsilon_{0t}/3 = 0.02$ of volumetric transformation strain, because the radial expansion ε_{tr} at the interface does not experience resistance of the solid. That is why in Ref. 4 the radial transformation strain was assumed as the limit case. Here, we found that for relatively large particles with $R > 10\,\mu$m, the maximum $\varepsilon_{t\phi} = 0.018$—i.e., almost the entire total tangential strain relaxes. At the same time, for particles with $R = 5$ and 3 nm, which are under essential pressure due to surface tension, the maximum $\varepsilon_{t\phi} = 0.0065$ and 0.001 only, respectively. That is why internal stress relaxation is not essential and does not affect θ_m.

In Fig. 1(b), the thickness h of the surface molten layer is plotted versus $\theta_e - \theta$. For $R \leqslant 5$ nm, the results based on the models with and without stress relaxation are very close. For $R \simeq 20$ nm, the difference in h is large. For $R \geqslant 40$ nm, the curves differ qualitatively. While for the plane interface the results from the model with deviatoric strain are in good agreement with experimental data, results for $\Lambda = 0$ even show saturation (rather than divergence) in h and differ qualitatively from experiments.

In Fig. 2, the distribution of radial σ_r and tangential σ_ϕ stresses with different values of Λ are shown. The dot in

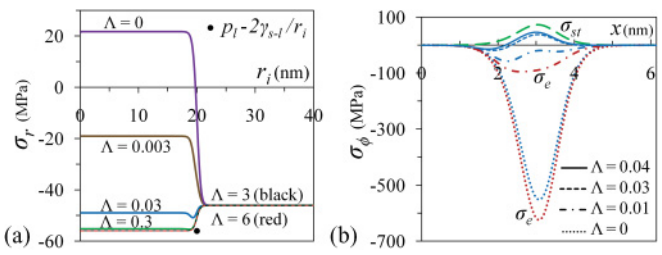

FIG. 2. (Color online) (a) Distributions of radial stresses in an Al particle with $R = 40$ nm for an interface position $r_i = 20$ nm at $\theta = \theta_e$ for different values of Λ. The dot corresponds to the pressure in the solid calculated with the Laplace equation $p_l - 2\gamma_{sl}/r_i$. (b) Distributions of tangential stress σ_ϕ and its elastic σ_e and surface tension σ_{st} contributions across the plane solid-melt interface at $\theta = \theta_e$. The surface tension σ_{st} [Eq. (5)] is the same for all cases. Four unmarked curves are for total stresses.

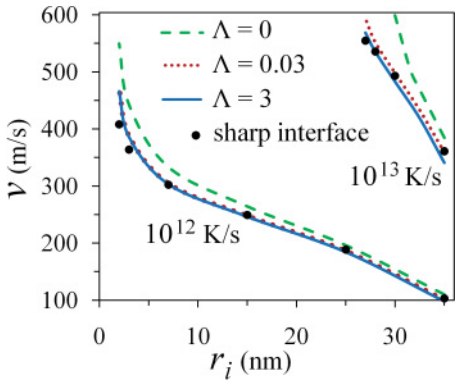

FIG. 3. (Color online) Interface velocity vs interface position for different heating rates and $\Lambda = 0$. The dots correspond to an analytical solution (Ref. 4). The two lowest curves for different Λ coincide.

Fig. 2(a) is for the pressure in a solid calculated with the Laplace equation $p_l - 2\gamma_{sl}/r_i$, which corresponds to the lack of elastic stresses (as for a liquid-liquid interface). Such pressure can be achieved for $\Lambda = 3$, and it does not change with a further increase in Λ. This value is two orders of magnitude larger than that required for independence of θ_m of Λ—i.e., a comparison of stress distribution with experiment or MD results is a much more sensitive method to determine Λ than a comparison with θ_m. The reason for the deviation from the Laplace equation is the elastic tangential stresses. At smaller values of Λ, the pressure jump reduces, then changes sign, and for $\Lambda = 0$ it even leads to tensile pressure in the solid core. At the same time, a realistic curve is shown between the curves for $\Lambda = 3 \times 10^{-2}$ (above which θ_m is independent of Λ) and $\Lambda = 3$—i.e., the results without a deviatoric transformation strain are completely inadequate.

In Fig. 2(b), distributions of tangential stress σ_ϕ and its elastic σ_e and surface tension σ_{st} contributions across the plane solid-melt interface are shown. For $\Lambda \geqslant 4$, σ_e completely relaxes, and the total stress coincides with the surface tension $\sigma_{\mathrm{st}} > 0$. Since volumetric transformational expansion generates compressive elastic tangential stresses σ_e, total tangential stress may be completely tensile, or compressive, or may vary from compressive to tensile stress while moving from a solid to melt, depending on the degree of relaxation of the elastic stresses. The plots of total tangential stresses in Fig. 2(b) reproduce typical stress distributions and the proper magnitude of plots for different crystal faces in MD

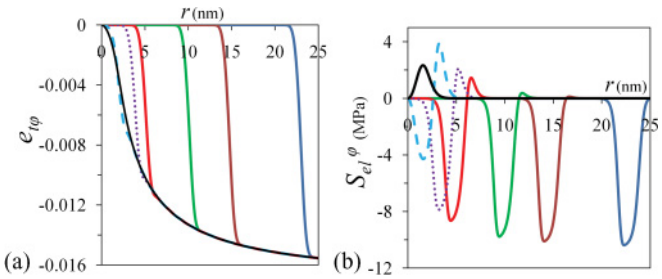

FIG. 4. (Color online) Tangential deviatoric transformation strain (a) and elastic stress (b) for $R = 40$ nm and $\Lambda = 0.04$, and $\theta = 930.8$ K at different interface positions.

simulations[1] and allow one to explain the reasons for such a variety and nontrivial shapes of the distributions. Note that the elastic stresses only contribute to GL Eq. (6); surface tension affects melting by changing the distribution of elastic stresses. For $\Lambda = 0$, the magnitude of compressive stresses is much larger than in MD simulations;[1] this causes an unrealistic increase in melting temperature above θ_e. The model of a coherent solid-melt interface with proper surface tension was introduced in Ref. 4, but only after introduction of stress relaxation and the ability to reproduce and explain typical stress distributions in MD simulations[1] can one claim the conceptual validity of this model.

Melting under a high heating rate and overheating are not only of fundamental interest, but also have an applied significance—e.g., for the melt-dispersion mechanism of the reaction of Al nanoparticles.[10] Interface velocities v are shown in Fig. 3 for two heating rates, 10^{12} and 10^{13} K/s. Due to the small particle size, the homogeneous temperature is justified.[10] For 10^{13} K/s, the interface propagation stops at $r_i = 25.9$ nm because homogeneous melt nucleation and reduction of η in the region $r_i < 25.9$ nm completes melting faster. An increase in Λ decreases the interface velocity, and the difference with the case with $\Lambda = 0$ is larger for a higher heating rate and smaller interface radii. The dots in Fig. 3 correspond to the analytical solution.[4]

Our results for $\Lambda = 3 \times 10^{-2}$ and 3 are close to each other and to the sharp-interface solution, while for $\Lambda = 0$ the interface velocity is significantly higher. The promoting effect of the elastic stresses on interface propagation (which confronts their suppressive effect on the initiation of melting) is consistent with the analytical solution,[4] i.e., to the linear relationship between v and the thermodynamic force for interface propagation per unit deformed volume of solid X, when internal stresses are neglected:

$$v = 6X\chi\sqrt{\beta\rho_m/(2A\rho_s)},$$
$$X = \frac{\rho_s}{\rho_{0s}} H\left(1 - \frac{\theta}{\theta_e}\right) + p_m\left(\frac{\rho_s}{\rho_m} - 1\right) - \frac{1}{2}\left(\frac{p_m^2}{K_m} - \frac{p_s^2}{K_s}\right) + \frac{2\gamma_{s-l}}{r_i}. \quad (8)$$

The elastic energy effectively increases γ_{s-l} and, consequently, the driving force. Note that the temperature at some points in Fig. 3 significantly (up to 200 K) exceeds the instability temperature of solid θ_i; still, the sharp interface approach gives good results.

In Fig. 4, the tangential deviatoric transformation strain and elastic stress are shown for $R = 40$ nm and different interface positions at $\theta = 930.8$ K. For all interfaces, there is a common curve characterizing residual deviatoric strain at each point after the interface passes through, and the major part of the curves for each specific interface position is above it. This results in compressive elastic deviatoric stresses with the maximum below 10 MPa. However, when the curve for an individual interface in Fig. 4(a) falls below the common curve, tensile deviatoric stresses appear in Fig. 4(b). With decreasing r_i, smaller deviatoric strain is required to reduce elastic stresses to the same and even a lower level.

In summary, an advanced GL model for the coherent solid-melt interface with a transformation strain tensor, the deviatoric part of which is described by a thermodynamically consistent kinetic equation, is developed. The corresponding relaxation of the elastic energy produces a promoting contribution to the driving force for phase transformation in the GL equation, both for melting and solidification. All types of interface stress distributions from known MD simulations are obtained as a combination of surface tension and elastic stresses with different degrees of relaxation. Without a deviatoric transformation strain, elastic stresses are overestimated by a factor of 5–10, which leads to qualitative contradictions in the size dependence of the melting temperature and the temperature dependence of the thickness of the surface molten layer. With the kinetic equation for $\boldsymbol{e}_t$, good agreement for both these relationships with experiments for Al nanosize and large-size particles is obtained. Results can be generalized for large strain using the methods developed in Ref. 11. A similar approach can be applied for sublimation and condensation,[12] amorphization and vitrification,[12] chemical reactions,[7] and other transformations for which $\boldsymbol{e}_t$ is not determined by geometry, both with and without the phase-field approach.

The support of NSF, AFOSR, and ARO is acknowledged.

[1] T. Frolov and Y. Mishin, Modell. Simul. Mater. Sci. Eng. **18**, 074003 (2010); Phys. Rev. B **82**, 174114 (2010).

[2] R. Lipowsky, Phys. Rev. Lett. **49**, 1575 (1982); J. Chang and E. Johnson, Philos. Mag. **85**, 3617 (2005).

[3] D. M. Anderson, G. B. McFadden, and A. A. Wheeler, Physica D **135**, 175 (2000); J. Lowengrub and L. Truskinovsky, Proc. R. Soc. London Ser. A **454**, 2617 (1998).

[4] V. I. Levitas and K. Samani, Nat. Commun. **2**, 284 (2011).

[5] J. Slutsker, K. Thornton, A. L. Roytburd, J. A. Warren, and G. B. McFadden, Phys. Rev. B **74**, 014103 (2006).

[6] M. A. Grinfeld, *Thermodynamic Methods in the Theory of Heterogeneous Systems* (Longman, Sussex, 1991); Dokl. Akad. Nauk SSSR **251**, 10 (1980).

[7] V. I. Levitas, V. F. Nesterenko, and M. A. Meyers, Acta Mater. **46**, 5929 (1998); V. I. Levitas, Int. J. Plasticity **16**, 805 (2000).

[8] S. L. Lai, J. R. A. Carlsson, and L. H. Allen, Appl. Phys. Lett. **72**, 1098 (1998).

[9] A. W. Denier van der Gon, R. J. Smith, J. M. Gay, D. OConnor, and J. van der Veen, Surf. Sci. **227**, 143 (1990).

[10] V. I. Levitas, B. W. Asay, S. F. Son, and M. Pantoya, J. Appl. Phys. **101**, 083524 (2007); V. I. Levitas, Combust.Flame, **156**, 543 (2009).

[11] V. I. Levitas and M. Javanbakht, Phys. Rev. Lett. **105**, 165701 (2010); V. I. Levitas, V. A. Levin, K. N. Zingerman, and E. I. Freiman, *ibid.* **103**, 025702 (2009); V. I. Levitas and D. Preston, Phys. Lett. A **343**, 32 (2005).

[12] V. I. Levitas and N. Altukhova, Phys. Rev. Lett. **101**, 145703 (2008); V. I. Levitas, *ibid.* **95**, 075701 (2005).